Effect of Mixing on the Precipitation of Barium Sulfate in an MSMPR Reactor

The effect of mixing intensity (power input) on the precipitation/crystallization of barium sulfate in a two-feedstream (sodium sulfate, barium chloride) continuous stirred-tank crystallizer with mixed product removal was investigated through experiments and companion mathematical models. Crystal growth rate and nucleation rate were very sensitive to mixing intensity, with growth rate increasing eightfold and nucleation rate decreasing 100-fold as power input per unit mass was increased from 0.001 to 0.73 m^2/s^3 (0 to 1,200 rpm stirrer speed). Experimental results at high feed concentration were accurately described by a model accounting for homogeneous nucleation and kinetic growth of particles as well as turbulent mass transfer to particles and turbulent micromixing of feedstreams. The principal mixing effect was due to particle mass transfer, not micromixing. Experiments at low feed concentration were more difficult to model because of a more complex nucleation mechanism and altered particle morphology.

David E. Fitchett
John M. Tarbell
Department of Chemical Engineering
Pennsylvania State University
University Park, PA 16802

Introduction

Crystallization is one of the oldest and most widely used of all industrial chemical operations. Crystallization from aqueous solution is a key production step for a wide range of products, such as fertilizers, sucrose, pharmaceuticals, and photographic films. Both physical and chemical interactions among solute, solvent, and solid are involved in reaction crystallization from aqueous solution, as suggested in Figure 1. The chemical processes of nucleation and growth have been widely studied (Randolph and Larson, 1971; Mullin, 1972), but much less systematic attention has been paid to the physical influences of hydrodynamics (mixing) on these chemical steps or the effects of solid crystal loading on the hydrodynamics. The purpose of the present investigation was to study the effect of mixing on the crystallization process in the absence of any feedback between the solids loading and the hydrodynamics, represented by dashed line in Figure 1. This uncoupling was achieved by running our crystallizer at relatively low levels of solids loading—less than 1% of volume.

In a simple reaction crystallization process involving two reactants, A and B, forming a supersaturated product, C, which precipitates out, mixing may alter the process in at least two plausible ways, as indicated in Figure 2. The reaction of A and B, which is typically thought to be exceedingly rapid, may be limited by the rate at which A and B are mixed at the molecular scale by the turbulence present (turbulent micromixing). In addition, the growth of crystals formed by precipitation may be limited by turbulent diffusion. The possible influences of mixing on the nucleation step appear to be more subtle. If primary homogeneous nucleation is dominant, then a direct mixing influence seems unlikely to be important, since the contacting of distinct species or phases is not involved and local supersaturation controls. However, primary heterogeneous nucleation or secondary nucleation, both of which involve fluid-solid contacting, are more likely to be sensitive to mixing. Models for the turbulent micromixing limitation and the turbulent diffusion limitation are presented later in this paper. The direct influence of mixing on nucleation will not be considered. Nonetheless, nucleation will be influenced indirectly by turbulent micromixing and diffusion to the extent that these processes control the level of supersaturation in the reactor.

We chose the precipitation of barium sulfate from aqueous feedstreams of barium chloride and sodium sulfate as our experimental chemical system. This system has been extensively studied, and nucleation and growth kinetics over a broad range of supersaturations are available (Nielsen, 1958, 1961, 1969). Barium sulfate is a sparingly soluble salt, and thus its nucleation is rapid and is generally believed to follow a primary homogeneous mechanism at high concentrations. The precipitations were carried out in a mixed suspension, mixed product removal (MSMPR) reactor operating in the steady state (Randolph and

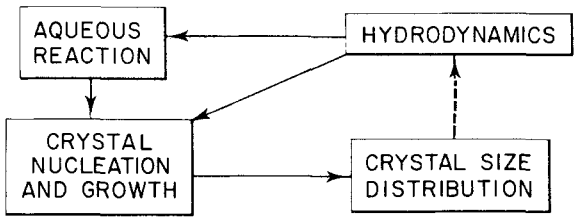

Figure 1. Physical and chemical interactions in liquid-solid precipitation/crystallization reactions.

Larson, 1971). The MSMPR reactor was chosen for these initial studies of the influence of mixing on crystallization because it is easy to characterize and analyze. However, we recognize at the outset that micromixing effects on homogeneous chemical reactions, such as $A + B \rightarrow C$ in Figure 2, are generally not as pronounced in continuous stirred-tank reactors as they are in plug flow or batch reactors (Chang et al., 1986).

We are aware of only two recent studies in which mixing effects in a continuous stirred-tank crystallizer were investigated. Garside and Tavare (1985) presented a theoretical analysis of certain limiting states of micromixing in an MSMPR crystallizer: I, maximum species mixedness–maximum age mixedness, and II, maximum species mixedness–minimum age mixedness. They did not consider intermediate age segregation or species segregation and did not model diffusion-limited particle growth. Pohorecki and Baldyga (1985) studied barium sulfate precipitation in a continuous stirred-tank crystallizer at several stirring speeds, feed concentrations, and residence times in ranges of the same order of magnitude as considered in the present study. They observed that mean particle size increased with stirrer speed (less than 50% increase for stirrer speeds between 60 and 360 rpm), and attributed this to a turbulent micromixing limitation in their modeling of the experiments. As we shall see, our experiments also show an increase in mean particle size with stirrer speed (up to an eightfold increase for stirrer speeds between 0 and 1,200 rpm), but we believe that turbulent diffusion-limited particle growth, not micromixing, is primarily responsible for the influence of stirrer speed on particle size in our experiments. We return to this point at the end of the paper. A few studies of mixing effects in semibatch crystallizers have also been reported (Nyvlt and Zacek, 1986; Pohorecki and Baldyga, 1983).

Experimental Methods

Barium chloride and sodium sulfate, both certified ACS grade (Fisher Scientific) were used to prepare the aqueous feedstreams. Single-distilled water was determined to be of sufficient purity for all experiments after precipitation tests using water of greater purity showed no difference in the crystal size distribution (CSD).

The experimental system used for the study is shown in Figure 3. It comprised a 1.8 L glass crystallizer with an acrylic plastic draft tube and baffle, a pair of 110 L feed tanks, high-capacity peristaltic feed pumps, rotameters, and filters for the barium sulfate feeds. All of the tubing used to integrate the system was 1.27 cm ID transparent Tygon tubing, except for a few experiments in which a small section of 0.48 cm ID Tygon tubing was connected at the end of each line feeding the crystallizer, to alter the feed jet velocity. Since the peristaltic pumps produced an oscillatory flow pattern at low flow rates, two recycle lines were installed so that the pumps could always be operated at near full capacity to reduce the oscillations. The feed rate was varied by adjustment of the recycle valves *A*. The valves labeled *B* were installed so that the feeds could be recycled through the filters before each experiment.

Gilmont shielded bypass flowmeters were used to monitor flow rates to the crystallizer. Each meter could measure flow rates between 1.3 and 9.4 L/min with an accuracy of ±0.05 L/min. Fin-L submicronic filters (Poly-Bio-Marine) were installed in each line to remove impurities from the feeds. These high-flow, high-performance filters utilized double filter bags capable of removing particles down to a nominal diameter of 0.65 μm at flow rates of up to 80 L/min with a pressure drop of only 0.5 psi.

The crystallizer is shown in Figure 4. It was fabricated by cutting a 3.0 cm wide rectangular weir in a 2,000 mL Pyrex beaker at a height of 13.5 cm above the base. The inside diameter of the beaker was 12.6 cm. A 5.5 cm length of 2.54 cm ID rubber tubing was secured below the weir as an outlet trough. This weir configuration resulted in crystallizer volumes of 1.7 to 1.8 L ±5% for the feed rates used in the experiments. The draft tube baffle was constructed entirely of 0.32 cm thick acrylic plastic. It consisted of three vertical baffles, separated by 120 degrees, glued to a cylindrical draft tube. A diameter of 8.2 cm

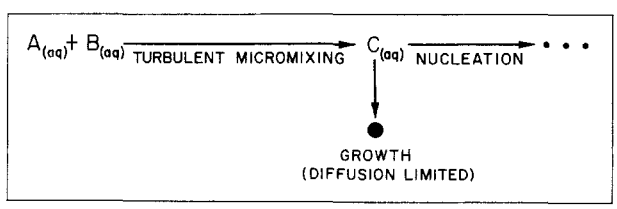

Figure 2. Effect of mixing in precipitation mechanism.

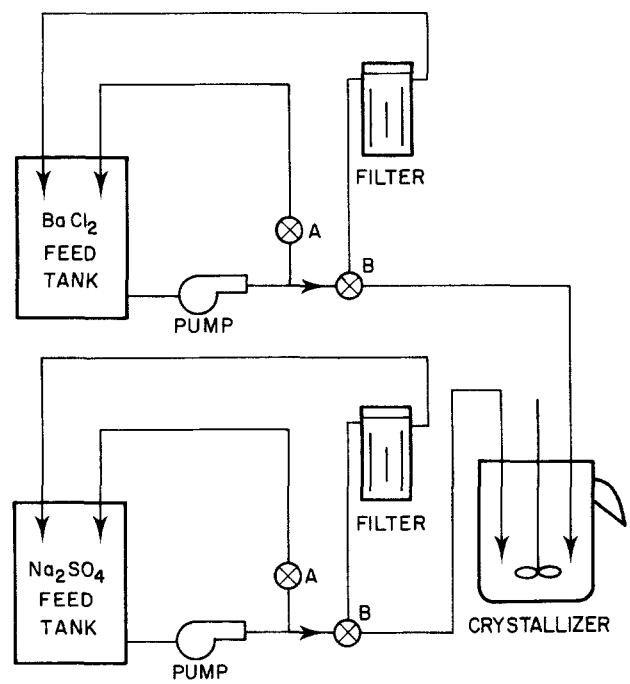

Figure 3. Experimental system.

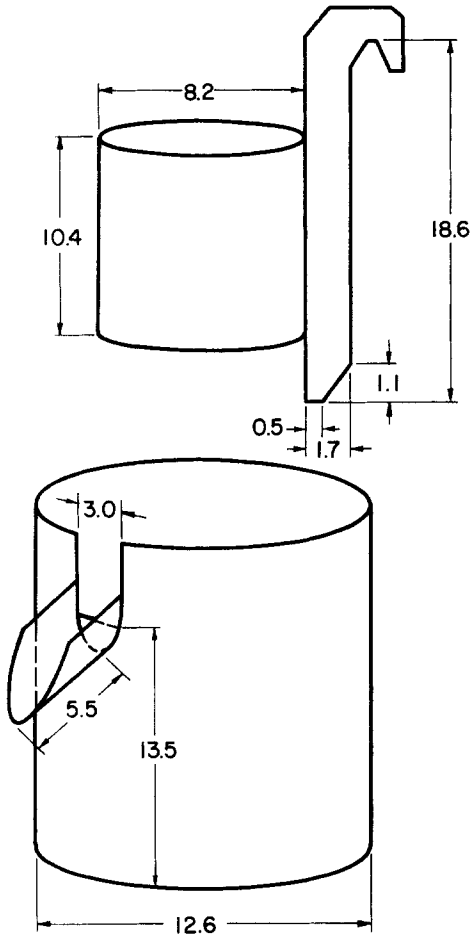

Figure 4. Crystallizer and draft tube baffle assembly.
Only one of three baffles shown, for clarity; all dimensions in cm

and a height of 10.4 cm were chosen for the draft tube so the cross-sectional area for flow around the tube was approximately constant. An acrylic plastic hook was attached to the top of each baffle so the draft tube baffle assembly hung inside the crystallizer approximately 0.3 cm from the wall and the bottom, leaving no corners along the crystallizer wall or bottom where particles could settle.

The crystallizer was agitated with a two-blade pitched paddle axial impeller which had a diameter of 4.0 cm, a height of 1.5 cm, and a pitch angle of 62 degrees. The impeller was positioned vertically down the central axis of the draft tube baffle with the bottom edge of its blade in the plane of the bottom edge of the draft tube. Its clockwise rotation (as viewed from the top) coupled with its blade orientation created an upward flow through the center of the draft tube and a corresponding downward flow in the annular section. This flow pattern permitted the use of high impeller speeds (1,200 rpm) without significant air entrainment or vortexing. During normal operation, the two feed tubes were positioned on opposite sides of the crystallizer in the annular section between the draft tube and the crystallizer wall with their outlets located in the plane of the bottom edge of the draft tube and pointing downward. The feed solutions were drawn directly into the impeller region by the macrocirculation pattern in the reactor.

The power input per unit mass of the impeller was determined by calorimetry. The crystallizer was insulated, equipped with a thermocouple, and loaded with a known mass of water. The rate of temperature rise was measured as a function of impeller speed and the power input per unit mass was calculated.

The experimental procedure involved setup of the system, operation of the crystallizer, and analysis of results. Preparation of the feed solutions was the most important part of the setup procedure because determination of feed concentrations was critical for duplication of experiments. For this task, a conductivity meter was calibrated using small batches of prepared solution and then used to determine the correct concentrations of the actual feed solutions. The feed concentrations of barium chloride and sodium sulfate were set equal for all experiments. The remainder of the setup procedure involved choosing experimental conditions, filtering the feeds, and calibrating the flowmeters.

Table 1 contains a list of all the experimental conditions studied, showing the range of residence times, feed concentrations, and impeller rotation rates. For each experiment a single feed rate (residence time) and feed concentration were used while several impeller speeds were employed. For tests of the effect of feed tube diameter variation, the tubes were changed in the middle of the experiments during a brief period in which the feed streams were recycled. Since several parameters were varied in this investigation, one set of experimental conditions was chosen as the basic operating state:

Postmix feed concentration = 0.15 M
Residence time = 38 s
Feed tube diameter = 1.27 cm

Experiments were performed by starting up the feed pumps, setting the impeller at the desired speed using a touch tachometer, waiting at least 15 residence times for steady state to be achieved in the crystallizer, and then taking samples of the crystallizer contents. Four to six impeller speeds were utilized during each experiment, and at least 15 residence times elapsed between changes in operating conditions and the onset of sampling. At least two samples were taken at each impeller speed and at least two residence times were allowed to elapse between samples to insure that steady state had been reached. Preliminary experiments in which samples were taken from the top and bottom of the reactor at impeller speeds of 0, 200, 400, and 850 rpm indicated that the CSD was independent of sample position. The power input from the feed jets was enough to suspend and disperse the particles even in the absence of stirring. Therefore, samples were taken from the same position for all experiments (draft tube region, midway between the impeller shaft and draft tube wall, and about two-thirds of the way up the draft tube).

Samples were obtained using a 1.0 mL capacity automatic micropipet which was adjusted to full capacity at all times. First, the pipet tip was inserted into the crystallizer magma; then the 1.0 mL sample was quickly and carefully drawn into the tip and quickly transferred to a breaker containing 400 to 500 mL of dilution medium to quench the reaction. The sampling process took about one second. The dilution medium was made by mixing enough barium chloride and sodium sulfate to create a saturated barium sulfate solution and then filtering it though a 1.0 μm polycarbonate membrane to remove impurities and precipitated barium sulfate. This solution preserved the barium sulfate CSD during sampling as well as during subsequent dilution before analysis.

Table 1. Experiments and Values of System Parameters

Run No.*	C_{A0} M	τ s	D_F cm	Impeller Speed, rpm						
				0	200	400	750	850	950	1,200
8	0.15	18	1.27	X	—	X	—	X	—	—
9	0.15	9	1.27	X	—	X	X	X	—	—
12	0.05	38	1.27	X	X	X	—	X	—	—
13	0.01	38	1.27	X	X	X	—	X	X	—
14	0.15	38	1.27	X	X	X	—	X	X	—
15	0.15	38	0.48	X	X	X	—	—	X	—
15	0.15	38	1.27	X	X	X	—	—	X	—
16	0.15	26	1.27	X	X	X	X	—	X	X
17	0.15	9	1.27	X	X	X	—	—	X	X
18	0.05	38	1.27	X	X	X	X	—	X	X
19	0.01	38	1.27	X	X	X	X	—	—	X
20	0.15	38	0.48	X	X	X	X	—	—	X
20	0.15	38	1.27	X	—	—	—	—	—	X
21	0.15	9	1.27	X	—	X	—	X	X	X
22	0.15	18	1.27	X	—	X	X	—	—	X
23	0.15	26	1.27	X	—	X	—	X	—	X
24	0.15	38	1.27	X	—	X	X	—	—	X

Runs 1–7 were preliminary experiments. Run 10 was omitted because of faulty experimental procedure. Run 11 was an experiment to test the effect of feed tube position on CSD. Feed tube diameter was changed during Runs 15 and 20.

Following each experiment, the samples were analyzed using a Hiac/Royco model 4300 particle size distribution analysis system equipped with a Hiac/Royco Model ASAP aspirating sampler and a model CMH-150 high particle concentration sensor. The sensor uses an optical shadowing principle to size particles. This sensor was specified for particles in the 2.5 to 150 μm range at densities of 4,000 particles per mL and flow rates of 50 mL/min. Dilution factors of 4,000 to 50,000, depending on the feed concentration and mixing rate, were required to meet the counting capacity of the Hiac/Royco system. The convention established for sample analysis was to make two or three consecutive one-minute (50 mL) counts on each diluted sample and average the results. Size distribution data were then graphed on semilog plots and crystal nucleation and growth rates were calculated using the MSMPR model (Randolph and Larsen, 1971).

In addition to size distribution analysis, crystal morphology was studied using a scanning electron microscope (SEM). Beginning with run 15, two specimens from each experiment (four from run 20) were prepared for SEM observation and photographs. One specimen was chosen from a sample taken at the highest impeller speed and one from a sample taken at the lowest impeller speed. A specimen was prepared by placing a drop of diluted sample on an aluminum specimen disk and allowing it to dry in a dessicator before coating it with a thin layer of gold to improve heat conductivity, thus enhancing photographic quality. The photographs of the particles were used to characterize particle morphology.

Results

The parameters varies in this investigation were power input, residence time, and feed concentration. The power input was altered within each experiment through variation of impeller speed. In addition, the power input from the feeds was varied by the use of different feed tube diameters. There was a small additional variation of power input caused by differences in feed rates at different residence times. The maximum power input per unit mass delivered to the reactor was about 0.75 m^2/s^3. The four residence times investigated were 9, 18, 26, and 38 s. Short residence times were necessary to investigate micromixing effects which, as shown by Eq. 16, occur on a time scale of at most a few seconds. The three postmix feed concentrations studied were 0.01, 0.05, and 0.15 M. The results displayed in this section are mean crystal length and nucleation rate as a function of power input per unit mass, with residence time and postmix feed concentration as parameters. In addition, SEM photographs are presented to characterize the crystal morphology.

The power that was the source of turbulent mixing in the crystallizer entered the system through both the feed tubes and the impeller.

$$P = P_{feed} + P_{imp} \tag{1}$$

Although the magnitude of P_{feed} was generally much smaller than P_{imp}, it was significant at the lower impeller speeds and shorter residence times. The magnitude of this contribution is given by

$$P_{feed} = \rho Q V^2 \tag{2}$$

where ρ is the fluid density, Q is the feed tube flow rate, and V is the mean velocity Q/S.

P_{imp} was calculated from the power number,

$$P_0 \equiv \frac{P_{imp} g}{\rho \mu^3 d^5} \tag{3}$$

where g is the gravitational acceleration, μ is the fluid viscosity, and d is the impeller diameter. Our calorimetry experiments showed P_0 to be independent of impeller speed, but to vary between 1.40 and 1.70 in several experimental trials. We used

an average value of $P_0 = 1.52$ for all calculations of P_{imp}. This value of P_0 is in close agreement with that predicted by a correlation of Vlcek et al. (1979) for a similar reactor with draft tube.

The nucleation rate, B^0, and growth rate, G, of the crystallization system were determined from the measured crystal size distributions (CSD) with the aid of Randolph and Larson's idealized MSMPR theory (size-independent growth), which predicts the following exponential CSD:

$$n = n^0 \exp\left(\frac{-L}{G\tau}\right) \tag{4}$$

where n is the number density, L is the particle length, G is the growth rate, τ is the residence time, and n^0 is the number density of nuclei.

A semilog plot of n versus L should yield a straight line having a slope, $-1/G\tau$, and an intercept, n^0, for a system following the simple MSMPR theory. Figure 5 shows the semilog (MSMPR) plots for the data of run 15. It conforms extremely well to the MSMPR theory for all power input levels, as do all the data obtained in the experiments listed in Table 1. Note that the slope (α $1/G$) and the intercept (n^0) depend markedly on P. The smallest particle length reported in Figure 5 is 7 μm, which is based on particle counts between 6 and 8 μm. We were unable to obtain reliable particle counts at smaller sizes. The largest particle lengths reported were limited by the number of particle counts required to obtain statistical validity, at least 100.

Knowing n^0 and G, it is then possible to calculate the nucleation rate,

$$B^0 = n^0 G \tag{5}$$

the mean particle length,

$$\overline{L} = G\tau \tag{6}$$

the total number of crystals (per unit volume),

$$N_T = B^0 \tau \tag{7}$$

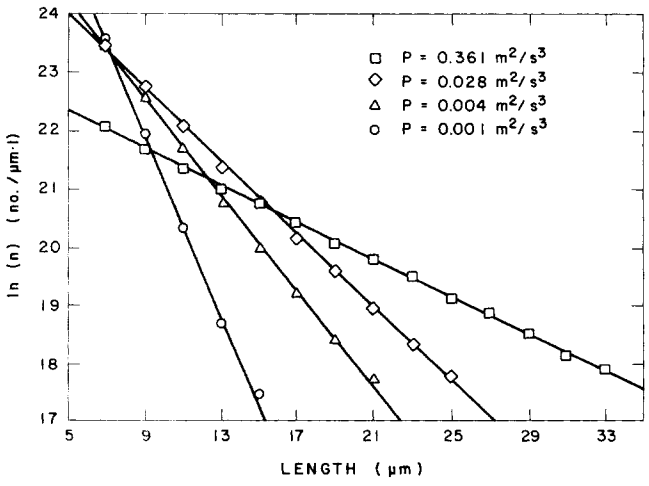

Figure 5. Typical MSMPR plot, run 15, at four power levels.

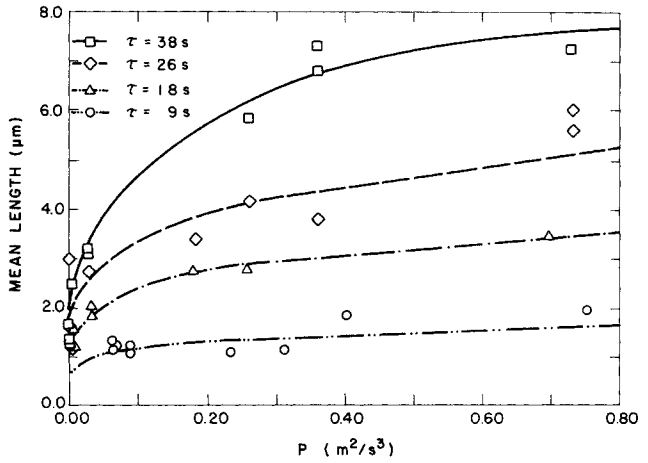

Figure 6. Mean particle length as a function of power input per unit mass at four residence times.
$C_{AO} = 0.15$ M, $D_T = 1.27$ cm

and the magma density (mass of crystals per unit volume)

$$M_T = 6k_V \rho B^0 G^3 \tau^4 \tag{8}$$

where k_V is a volume shape factor ($=\pi/6$ for spheres).

The effects of power input on crystal size and nucleation are presented in Figures 6 and 7, respectively. Experiments were performed at residence times of 9, 18, 26 and 38 s with the other operating parameters at their base values. Figure 6 is a linear plot of mean particle length versus power input per unit mass; Figure 7 is a semilog plot of nucleation rate versus power input per unit mass. Several important points should be noted in these figures.

The most significant trends are that mean particle length increased with increasing power input while nucleation rate decreased. These trends were most evident at the longest residence time, where the mean particle length increased by a factor of about eight and the nucleation rate decreased by over two orders of magnitude as the power input increased from near

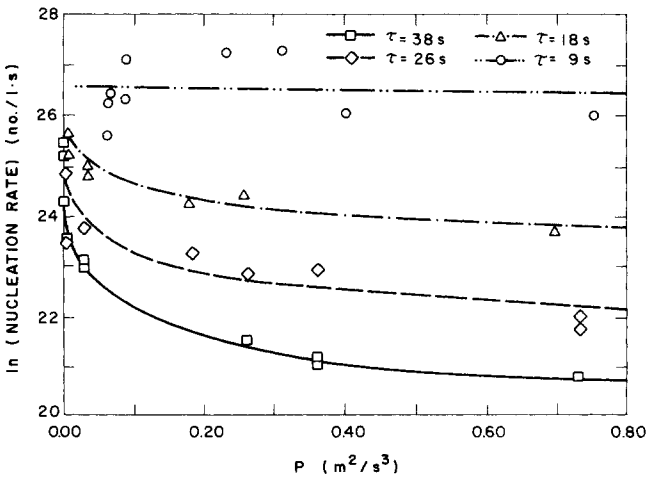

Figure 7. Nucleation rate as a function of power input per unit mass at four residence times.
$C_{AO} = 0.15$ M, $D_T = 1.27$ cm

zero to over 0.73 m^2/s^3. It should be kept in mind that the supersaturation level in the reactor was not held constant during these experiments even though the feed concentration was constant. A simple qualitative explanation of the observed trends is that at longer residence times, increased crystal growth reduces supersaturation, which in turn reduces nucleation rate. The growth rate itself, which is shown in Figure 8, is not markedly affected by residence time because it displays a much weaker dependence of supersaturation than does the nucleation rate; see Eqs. 18c and 22.

The data in Figures 6–8 exhibit a strong dependence on P at low levels and a tendency to become independent of P at high levels. This trend suggests either a micromixing limitation or a particle mass transfer limitation at low P. We return to this point later in the data analysis.

Figures 6–8 also give an indication of the reproducibility of the experiments since each set of data at a particular condition contains results from at least two experiments. There was some scatter in the data, primarily because the experiments were performed at relatively short residence times and high feed concentrations, which tend to increase the potential for sampling error. Indeed, the largest scatter in the nucleation and growth data is apparent at the shortest residence time.

Figures 9 and 10 show mean length and nucleation rate versus power input for feed concentrations of 0.01, 0.05, and 0.15 M with other operating parameters at their base values. Although the data show certain trends that are similar to those shown in Figures 6 and 7, there are some significant differences. Most notable is that the mean particle length reached a maximum value of approximately 8 μm at a P of 0.05 m^2/s^3 for the 0.01 M experiments and nearly the same maximum at a P of 0.2 m^2/s^3 for the 0.05 M experiments. A maximum was not observed at the highest concentration, but we believe it would be at higher power inputs beyond the range of our experiments. Thus, at the lower concentrations, beyond a certain intermediate P level, particle growth rate no longer increased with increasing power input. A similar phenomenon was observed by Koros et al. (1972) for NaCl crystallization in an MSMPR. They suggested that it was the result of a transition from mixing-controlled (mass transfer limited) growth to surface reaction controlled

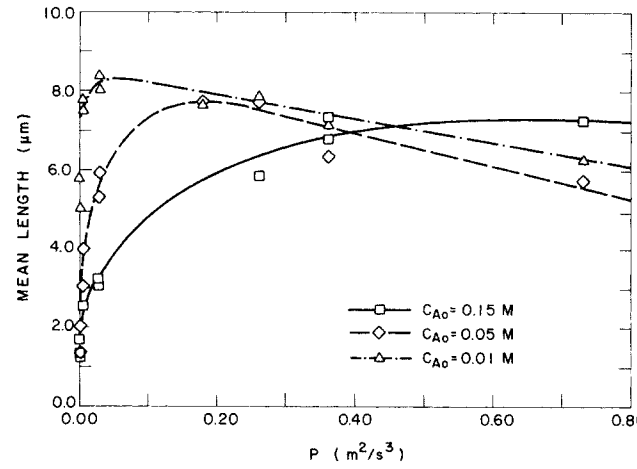

Figure 9. Mean particle length as a function of power input per unit mass at three feed concentrations.

$\tau = 38$ s, $D_F = 1.27$ cm

(kinetically limited) growth as power was increased. The decrease in mean particle length with increasing power input after the maximum had been reached was also observed by Koros et al. They suggested that it was a result of particle attrition that occurred at the highest mixing rates.

Overall, the data in Figures 9 and 10 are at least qualitatively consistent with a mixing-limited crystallization process. That is, kinetic nucleation and growth rates are expected to be reduced at lower feed concentrations, and thus the regime of kinetic control should be reached at lower power levels, as observed.

We should also point out that during experiments run with $C_{A0} = 0.01$ M, barium sulfate precipitate accumulated on the draft tube, baffle, and crystallizer walls. The accumulation was slightly less for experiments with $C_{A0} = 0.05$ M and insignificant for $C_{A0} = 0.15$ M. These observations suggest that the mechanism of nucleation at $C_{A0} = 0.01$ and 0.05 M differed significantly from the mechanism of 0.15 M. We return to this point in the section on modeling.

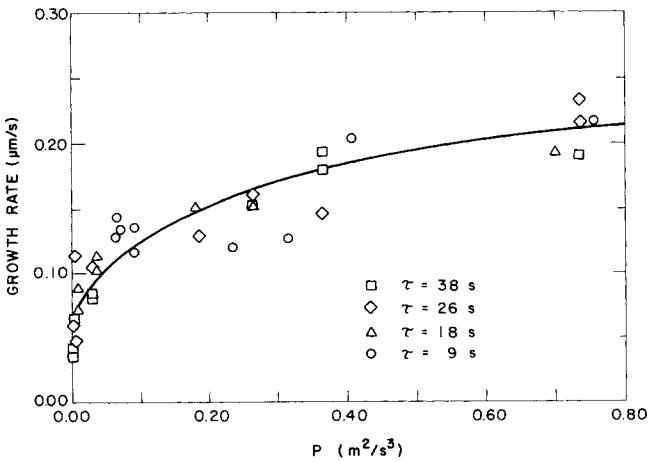

Figure 8. Growth rate as a function of power input per unit mass at four residence times.

$C_{A0} = 0.15$ M, $D_F = 1.27$ cm

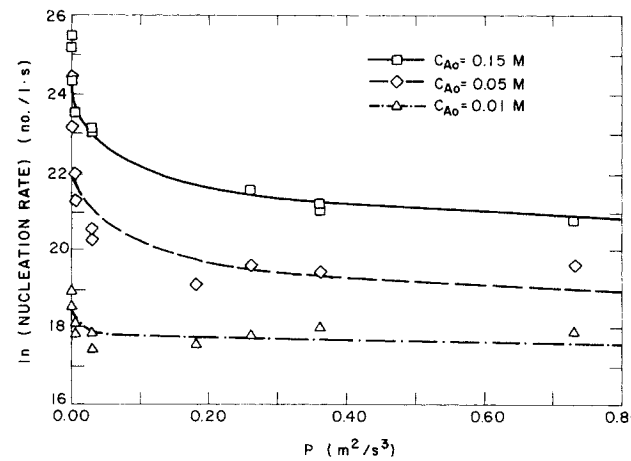

Figure 10. Nucleation rate as a function of power input per unit mass at three feed concentrations.

$\tau = 38$ s, $D_F = 1.27$ cm

To aid in the interpretation of our results, SEM photographs of particles from three experiments are displayed in Figure 11. There did not appear to be a significant influence of power level on morphology at any feed concentration, thus the principal influence displayed in Figure 11 is that of feed concentration.

Figure 11a is a particle characteristic of the 0.01 M feed concentration. It has an orderly dendritic structure with sharp edges; a dominant base plate with four branches; and a distribution of smaller dendrites jutting out of the base plate with a predominantly orthogonal orientation. Similar morphologies were reported by Takiyama (1958) and Dimitt and Graham (1976) for batch crystallizations at 0.001 and 0.002 M, respectively. A particle formed in a reactor with 0.05 M feed concentration is shown in Figure 11b. It too has a predominant base plate with some remnant of the four branches; evidence of dendritic structure; and a few orthogonal plates. However, it has rounder edges and a less orderly overall appearance. At a feed concentration of 0.15 M, Figure 11c, the particle no longer has a base plate, but rather consists of smooth-edged platelets that are joined by edge contacts. The platelets retain the predominantly orthogonal orientation displayed at lower concentrations, but there is no dominant base plate.

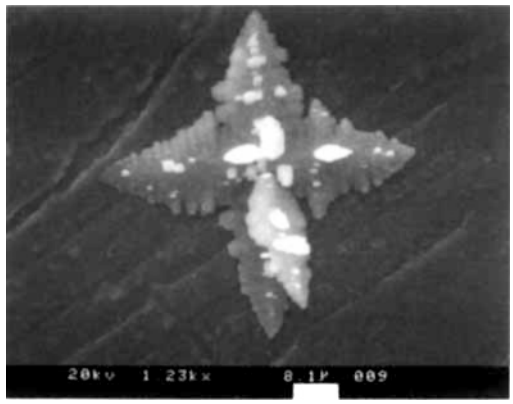

a. $C_{AO} = 0.01$ M, $\tau = 38$ s, $P = 0.001$ m^2/s^3

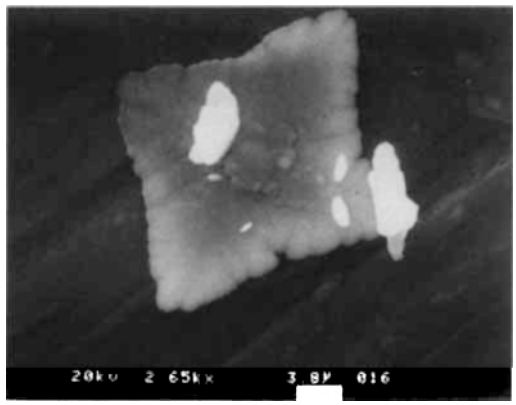

b. $C_{AO} = 0.05$ M, $\tau = 38$ s, $P = 0.731$ m^2/s^3

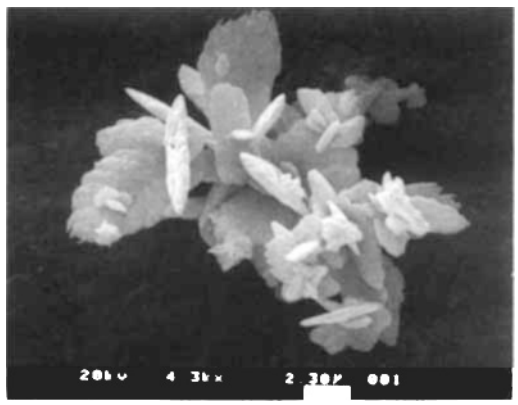

c. $C_{AO} = 0.15$ M, $\tau = 38$ s, $P = 0.731$ m^2/s^3

Figure 11. Scanning electron micrographs of typical barium sulfate particles at three feed concentrations.

The multiplatelet particles produced at a feed concentration of 0.15 M may at first glance appear to have been formed by platelet agglomeration. We do not believe this to be the case for several reasons:

1. The multiplatelet morphology was independent of the reactor stirrer speed
2. The orthogonal edge contacts are not characteristic of agglomerative systems (Lamey and Ring, 1986)
3. The MSMPR plots, Figure 6, were linear, whereas they are decidedly nonlinear in agglomerative systems (Beckman and Farmer, 1987)

Nonetheless, to further test for the possibility of agglomeration in our system we conducted a series of experiments at 0.15 M feed concentration and base state operating conditions after the addition of up to 5% gelatin (Knox Gelatine, average MW = 124,600) to the feedstreams of the reactor. Gelatin, at this concentration or lower, is used commonly to prevent particle aggregation during silver halide precipitation processes (Berriman, 1964). Our barium sulfate particles formed in the presence of gelatin displayed essentially the same morphology as observed earlier in the absence of gelatin, Figure 11c—multiplatelet structures with edge contacts. Thus, we believe that particle agglomeration is not a significant mechanism in our studies.

Mathematical Modeling

A definition sketch for the crystallizer is provided in Figure 12. Separate aqueous feedstreams of $BaCl_2$ (A) and Na_2SO_4 (B) are fed to the reactor at (mixed) concentrations C_{A0} and C_{B0}, respectively. The system is well mixed (macro-mixed) and the outlet stream contains $BaSO_4$ (C) in the liquid phase at concentration C_c and in the solid phase at concentration M_T (magma density). C_A and C_B are the liquid phase concentrations of unconverted A and B; Q is the volumetric flow rate; and V is the reactor volume. We assume that the reaction between A and B to form C, Figure 2, is bimolecular with rate constant k:

$$r = kC_AC_B \tag{9}$$

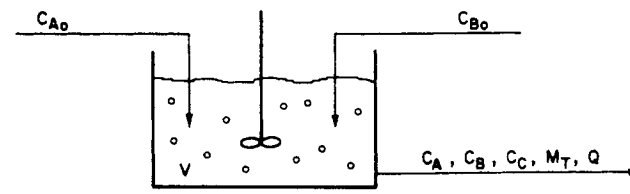

Figure 12. Definition sketch for crystallizer model.

We will use an apparent rate constant approach to describe the turbulent micromixing of A and B.

A component material balance on species A takes the form

$$Q(C_{A0} - C_A) - VkC_AC_B = 0 \tag{10}$$

For equimolar feed conditions, $C_A = C_B$, and therefore,

$$C_A = \frac{(-1 + \sqrt{1 + 4\tau kC_{A0}})}{2\tau k} \tag{11}$$

where $\tau = V/Q$ is the mean residence time of the reactor. A component balance on the product, C, leads to

$$-Q(C_C + M_T) + VkC_AC_B = 0 \tag{12}$$

and addition of Eqs. 10 and 12 results in

$$C_{A0} - C_A - C_C - M_T = 0 \tag{13}$$

which, along with Eq. 11, is the overall material balance for the reactor. In a perfectly micromixed reactor, one expects $k \rightarrow \infty$, and therefore $C_A \rightarrow 0$. In this limiting condition (perfect micromixing), the overall material balance reduces to

$$C_{A0} - C_C - M_T = 0 \tag{14}$$

which is the standard MSMPR material balance (Randolph and Larson, 1971).

To describe turbulent micromixing of A and B, we will use the apparent rate constant approach of Vassilatos and Toor (1965). In this approach, one sets the rate constant in Eq. 9 as follows:

$$k = k_{app} = \frac{1}{C_{A0}\tau_m} \tag{15}$$

where τ_m is the turbulent micromixing time constant, which can be estimated from Corrsin's theory (Corrsin, 1957):

$$\tau_m = 3.2\left(\frac{L_S^2}{P}\right)^{1/3} \tag{16}$$

Here, L_S is the integral length scale of the reactor and P is the total power input per unit mass added to the system. This expression has been shown to be very useful in modeling turbulent mixing and reaction experiments (Mehta and Tarbell, 1983; Tarbell and Mehta, 1986). In the present study, L_S is taken as the distance between the tip of the impeller blade and the draft tube (0.0225 m), as suggested by Mehta and Tarbell (1983). The value of P was calculated as described previously. The largest value of τ_m for any operating state of our experiments was $\tau_m = 2.8$ s for zero agitation speed and $\tau = 38$ s.

The micromixing model described above is about the simplest model available. We feel that it is an appropriate choice for the crystallizer because most of the available micromixing models do a good job of describing micromixing limitations on a single reaction ($A + B \rightarrow C$), as has been demonstrated by Chang et al. (1986) and Villermaux (1983).

Returning to the overall material balance, Eq. 13, we see that M_T must be expressed in terms of C_c in order to close off the system of equations. The required relation comes from the standard MSMPR theory based on the exponential distribution of particle sizes such as we have observed experimentally,

$$M_T = 6k_V\rho B^0G^3\tau^4 \tag{17}$$

where $B^0 = B^0(C_c)$ and $G = G(C_c)$.

$B^0(C_c)$ comes from the exhaustive experiment work of Nielsen (1961, 1969)

$$B^0 = 1.6 \times 10^{16}(C_c - C_c^*)^{2.7} \qquad (C_c - C_c^*) < 2.5 \times 10^{-4}\,M \tag{18a}$$

$$B^0 = 3.4 \times 10^{11}(C_c - C_c^*)^{1.4} \qquad 2.5 \times 10^{-4}\,M < (C_c - C_c^*) < 0.013\,M \tag{18b}$$

$$B^0 = 5.0 \times 10^{42}(C_c - C_c^*)^{18} \qquad (C_c - C_c^*) > 0.013\,M \tag{18c}$$

where C_c^* is the saturation concentration of C ($C_c^* = 9.5 \times 10^{-6}$ mol $\cdot$ L^{-1}). Note that nucleation appears to proceed by different mechanisms at different levels of supersaturation. The extremely high exponent of the supersaturation in the highest concentration range is indicative of a primary, homogeneous nucleation mechanism.

Particle growth is described by a two-step mechanism (Karpinski, 1985) involving turbulent transport of supersaturated aqueous barium sulfate to a particle surface followed by a chemical incorporation step at the surface. The rate of turbulent mass transfer from the bulk solution to a single particle surface is expressed as follows:

$$\frac{dm}{dt} = k_DA_C(C_c - C_{ci}) \tag{19}$$

In Eq. 19, m is the particle mass, k_D is the mass transfer coefficient, A_c is the particle surface area, and C_c and C_{ci} are the concentrations of C in the bulk solution and at the liquid-solid interface, respectively. The chemical incorporation step at the surface is described by

$$\frac{dm}{dt} = k_RA_c(C_{ci} - C_c^*)^r \tag{20}$$

where k_R is the rate constant for the surface reaction and r is the order of the concentration dependence (typically greater than 1).

The linear growth rate, G, is introduced by the relationship

$$A_c^{-1}\frac{dm}{dt} = \frac{3k_V}{k_A}\rho G \tag{21}$$

where k_V and k_A are the volume and area shape factors, respectively, and ρ is the particle density, 4,500 kg $\cdot$ m^{-3}. Eliminating C_{ci} between Eqs. 19 and 20 and introducing Eq. 21, we arrive at the final growth equation to be utilized in the model:

$$C_c - C_c^* = \frac{3k_V\rho G}{k_Ak_D} + \left(\frac{3k_V\rho G}{k_Ak_R}\right)^{1/r} \tag{22}$$

The growth kinetics of Nielsen (1958) will be incorporated ($r = 4$, $k_R = 6.3 \times 10^{11}$ $\mu m \cdot s^{-1} \cdot M^{-4}$). The particle mass transfer coefficient, k_D, will be treated as an adjustable parameter to fit the experimental data.

The values of k_V and k_A depend on the particle morphology and will vary with the reactor feed concentration. Most of our modeling effort has focused on the experiments at high feed concentration ($C_{A0} = 0.15$ M), and the discussion here is based on that case. We have set k_V so that the magma density calculated by Eq. 17 using experimentally determined values of B^0 and G would match the feed concentration ($M_T \sim C_{A0}$). This, of course, assumes a high conversion to solids, a state that is confirmed by subsequent model calculations. The resulting average value of k_V for the entire data set ($C_{A0} = 0.15$ M) is 0.06. This is much lower than the value for spheres ($\pi/6$), but not unexpected in light of the particle morphology, Figure 11c, which is not space filling.

Mullin (1972) has suggested that values for the ratio of k_A to k_V, denoted F, range from 6 for spheres and cubes to 10 for comminuted solids and much higher values for flakes and platelike crystals. We have chosen a value of $F = 10$ for our high concentration runs ($C_{A0} = 0.15$ M).

The mass transfer coefficient, k_D, will be related to the power input per unit mass, P, by a correlation of the form

$$Sh = BRe_p^a Sc^{1/3} \tag{23}$$

where the Sherwood, Schmidt, and particle Reynolds numbers are defined as follows:

$$Sh = \frac{k_D \bar{L}}{D} \tag{24}$$

$$Sc = \frac{\mu}{\rho_{sol} D} \tag{25}$$

$$Re_p = \frac{\epsilon^{1/3} \bar{L}^{4/3} \rho_{sol}}{\mu} \tag{26}$$

In the above equations, D is the diffusivity of barium sulfate; μ is the viscosity of the solution; ρ_{sol} is the density of the solution; $\bar{L}$ is the mean particle length; and ϵ is the rate of dissipation of turbulent energy in the crystallizer, which we equate with P.

The particle Reynolds number defined above is based on the Kolmogorov length scale of the turbulence and is an appropriate correlating parameter for mass transfer to particles that are smaller than the Kolmogorov length scale (Armenante and Kirwan, 1989),

$$\eta = (\nu^3/\epsilon)^{1/4} \tag{27}$$

where ν is the fluid kinematic viscosity. At the highest power inputs in our study, $\eta \sim 50$ μm, which is much larger than the mean particle lengths observed in our experiments.

The viscosity and density of the fairly dilute particulate solutions (less than 1% solids) are given accurately by the pure liquid values ($\mu = 10^{-3}$ kg $\cdot$ m^{-1} $\cdot$ s^{-1}; $\rho_{sol} = 1{,}100$ kg $\cdot$ m^{-3}), but the diffusivity of barium sulfate is not known with confidence. We will use a value of $D = 9.55 \times 10^{-10}$ m^2 $\cdot$ s^{-1} reported by Nielsen (1969). Thus, the values of the Schmidt number and the Sherwood number are only approximate. This is not critical since B, Eq. 23, is an adjustable parameter in our model. It should also be noted that we have not tested the exponent on the Schmidt number, as Sc is expected to be approximately constant over the range of our experiments. However, Re_p does vary significantly (0.001–0.139), and its exponent must be determined.

The entire mathematical model contains two adjustable parameters, B, a, that define the mass transfer coefficient correlation, and four unknown variables—C_c, B^0, G, M_T—that are determined by solution of the model equations. Two of the predicted variables, B^0 and G, can be compared to experimental measurements, Figures 7 and 8.

Comparison of Model and Experiment

Figures 13 and 14 provide a comparison of the experimental data and the model predictions for the high feed concentration runs both with and without the micromixing limitation included in the model. Perfect micromixing is achieved by setting $k_{app} \rightarrow \infty$. It is apparent that the mean length (or equivalently, the growth rate) and the nucleation rate are predicted quite accurately over the entire range of residence times and power inputs (mass transfer coefficients). The values of the adjustable parameters utilized to produce Figures 13 and 14 are

$$B = 0.26, \qquad a = 0.74 \tag{28}$$

The Sherwood numbers calculated by Eq. 23 using these parameters, Eq. 28, do not exceed a value of 0.62 at the highest Re_p of the experiments. Since one typically expects Sh to approach a lower limiting value of 2.0 for spherical particles in the absence of convection (Armenante and Kirwin, 1989), there may seem to be a contradiction in our results. However, our particles are not spherical; see Figure 11c. They consist of many platelets with edge contacts, and each platelet has a large aspect ratio (platelet extent divided by platelet thickness). As the aspect ratio of a particle approaches infinity, the limiting value

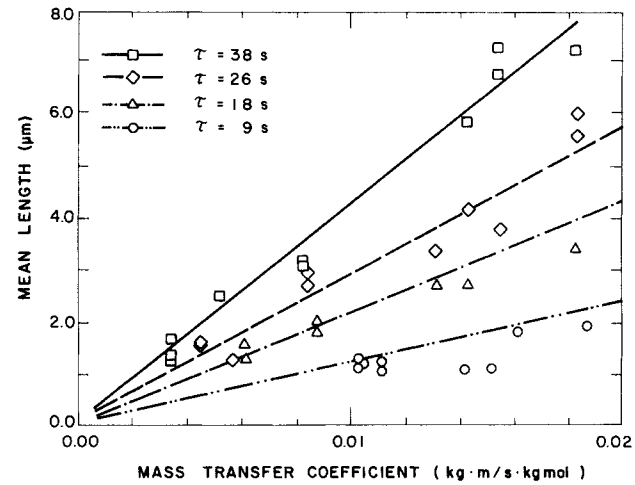

Figure 13. Mean particle length as a function of particle mass transfer coefficient at four residence times.

$C_{A0} = 0.15$ M, $D_T = 1.27$ cm
Symbols = data points; lines = model predictions, with and without micromixing limitation

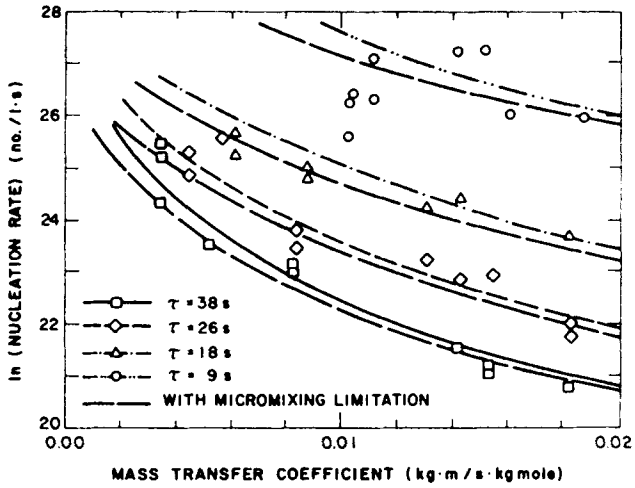

Figure 14. Nucleation rate as a function of particle mass transfer coefficient at four residence times.

C_{A0} = 0.15 M, D_F = 1.27 cm
Symbols = data points; lines = predictions without micromixing limitation
— — — model prediction with micromixing limitation

of Sh (diffusion limit) is expected to approach zero. This has been shown explicitly by Tsubouchi and Sato (1960) for prolate ellipsoids, which have an asymptotic value of $Sh = 2$ in the spherical limit (aspect ratio = 1) and $Sh = 0$ in the wire limit (aspect ratio = ∞). Thus it is not unreasonable to expect the limiting value of the Sherwood number for our particles to be considerably less than 2.

Figure 13 shows only one set of curves for both the perfect mixing and micromixing limited cases, indicating a negligible effect of micromixing on particle growth. The effect of micromixing on the nucleation rate is more pronounced—about a 25% reduction, Figure 14. The computer simulations showed that the micromixing limitation reduced the supersaturation in the reactor slightly, and this led to a reduction in the nucleation and growth rates. Because of its much stronger dependence on the level of supersaturation, the nucleation rate was influenced more strongly than the growth rate. It should be noted that the magma density is directly proportional to the nucleation rate, Eq. 8, and thus a 25% reduction in M_T, associated with the micromixing limitation, is predicted. Since the supersaturation is not affected greatly, the overall materal balance, Eq. 13, indicates that the reduction in M_T must be associated with an increase in unconverted reactant, C_A, of comparable magnitude to the decrease in M_T.

The exponent on the Reynolds number in the mass transfer correlation required to fit the model to the experimental data ($a = 0.74 \sim 3/4$) indicates, by way of Eqs. 23–26, that the mass transfer coefficient is independent of particle length. This is equivalent to McCabe's delta-L law (McCabe, 1929), which is one of the underlying assumptions of the classical MSMPR Model (Randolph and Larson, 1971). Straight MSMPR plots (e.g., Figure 5) are possible only when size-independent growth prevails. Thus, the value of the Reynolds number exponent in the mass transfer correlation is internally consistent with the observed MSMPR plots. It should also be noted that the Reynolds number exponent for mass transfer to particles in agitated tanks generally lies between 0.5 and 1.0 (Armenante and Kirwan, 1989). In addition, there are several theories of turbulent transport to particles that predict an exponent of 3/4 (Levich, 1962; Armenante and Kirwan, 1989) as well as experimental correlations that give the same value for the exponent (Sano et al. 1974).

One might argue that there are ways to correlate our experimental data other than to assume a particle mass transfer coefficient that depends on the agitation speed. For example, Pohorecki and Baldyga (1985) observed about a 50% increase in particle size with increasing agitation speed in the range of 60 to 360 rpm for $BaSO_4$ precipitation in a continous stirred-tank crystallizer, and they used a micromixing model without particle mass transfer limitation to predict the data. We have attempted to fit our data with a similar model by neglecting the particle mass transfer limitation and using the apparent rate constant, k_{app}, as an adjustable parameter. However, this model, although capable of predicting increases in particular size with increasing agitation speed, fails to simulate even the qualitative trends in the nucleation rate. It predicts an increase in nucleation rate with agitation rate, whereas the trend of the data, Figure 7, is clearly the opposite. The effect of improved micromixing at higher power input is to increase supersaturation, which in turn increases both growth and nucleation rates. However, when growth rate increases with power input through the mass transfer coefficient as we propose, supersaturation can be reduced, leading to a reduction in nucleation as observed.

It has also been suggested that the nucleation rate constant, k_B, might be dependent on the agitation rate if a secondary nucleation mechanism is really important. But this alone (i.e., with particle mass transfer coefficient independent of agitation) would lead to an increase in the nucleation rate and a decrease in the growth rate (supersaturation level) with increasing agitation speed, trends that are not borne out by the data.

Attempts to apply this model to the data with $C_{A0} = 0.01$ and 0.05 M have not been entirely satisfactory. Employing the same parameters that were successful in modeling the data at $C_{A0} = 0.15$ M to the lower concentration runs, we have been unable to predict the high growth rates in the low power input range (recall Figure 9). There are at least three factors that distinguish the lower feed concentration runs from the highest concentration runs that could alter the model:

1. The observed coating of the reactor and draft tube walls with precipitate at the lower feed concentrations suggests that a heterogeneous nucleation mechanism is operative. This type of nucleation is reactor dependent and would not have been accounted for in the experiments of Nielsen (1961), which provided the nucleation rate expressions that we have utilized in our modeling. The homogeneous nucleation mechanism that we applied to modeling the high concentration data, Eq. 18c, should be reactor independent.

2. In addition, the coating of the reactor suggests some form of particle death mechanism that we have not accounted for in our population balance. This, however, does not seem to be too important because our MSMPR plots were straight for all of the low feed concentration data. Death (and birth) terms usually lead to curvature of the MSMPR plot (Beckman and Farmer, 1987). Furthermore, the inclusion of a death term in a population balance would lead to the prediction of higher growth rates (at $C_{A0} = 0.01$ and 0.05 M) than already indicated in Figure 9 (note $G = \bar{L}_T$). But our problem in modeling is that the growth

rates at low feed concentration seem too high to begin with. Adding a death term makes them higher still.

3. There is a significant difference in the morphology of particles produced at low and high feed concentration, Figure 11. This suggests that the shape factors k_V and k_A might be different for the experiments at different feed concentrations. Since k_V was estimated to have a value of 0.06 for all experiments, this leaves k_A, or the rate $F = k_A/k_V$, as an adjustable parameter. Notice that the growth ratio, G, appears as G/F in Eq. 22. Mullin (1972) has indicated that F can be much greater than 10 for platelike crystals such as we have observed at the lower feed concentrations. Because of this we have carried out simulations using higher values of F for the lower feed concentration runs, and we are indeed able to shift the growth rates upward at low power inputs and bring the predictions into closer accord with the experiments (see Fitchett, 1988, for more details). However, the fit is not as good as what we have shown for $C_{A0} = 0.15$ M. We have not pursued the modeling of the low feed concentration experiments any further because of the complexity of the nucleation process under these conditions.

Conclusions

The model we have proposed assumes homogeneous nucleation, mass transfer limited particle growth, and micromixing-limited reaction between feed materials. It provides a very good fit to data with $C_{A0} = 0.15$ M over a broad range of power inputs and residence times. The parameters required to fit the model to the data are physically reasonable, and there is an internal consistency. At lower feed concentrations, a more complex nucleation mechanism and altered particle morphology make the prediction of data less satisfactory.

Acknowledgment

This work was supported by an Office of Naval Research FundamentalResearch Initiatives Contract. The authors thank W. S. Kim for carrying out the gelatin experiments and for critical review of the manuscript.

Notation

a = exponent, Eq. 23
A_c = surface area of crystal
B = constant, Eq. 23
B^0 = crystal nucleation rate
C = concentration
D = diffusion coefficient
D_F = feed tube diameter
G = linear growth rate
k = reaction rate constant
k_A = area shape factor
k_{app} = apparent reaction rate constant
k_D = mass transfer coefficient
k_R = surface reaction rate constant
k_V = volume shape factor
L = particle length
$\bar{L}$ = mean particle length
L_S = characteristic length in reactor
m = mass of a particle
M_T = magma density
n = number density of particles
n^0 = number density of particles at infinitesimal length
P = total power input
P_{feed} = power input from both feed streams
P_{imp} = power input from impeller
P_0 = power number
Q = volumetric flow rate
r = surface reaction order, or reaction rate
Re_p = particle Reynolds number
S = tube cross-sectional area
Sc = Schmidt number
Sh = Sherwood number
V = crystallizer volume

Greek letters

ϵ = turbulent energy dissipation rate
μ = viscosity
ν = kinematic viscosity
ρ = particle density
ρ_{sol} = solution density
τ = mean residence time
τ_m = micromixing time constant

Subscripts

A = reactant A
B = reactant B
C = product C
0 = postmix inlet concentration
i = concentration at interface between liquid and solid

Superscripts

$\hat{}$ = per unit mass
$*$ = saturation value

Literature Cited

Armenante, P. M., and D. J. Kirwan, "Mass Transfer to Microparticles in Agitated Systems," *Chem. Eng. Sci.*, **44,** 2781 (1989).

Beckman, J. R., and R. W. Farmer, "Bimodal Barite CSD Due to Agglomeration in an MSMPR Crystallizer," *AIChE Symp. Ser., 253, 85 (1987).*

Berriman, R. W., "Crystal Growth During the Formation of a Silver-Bromide Dispersion in Gelatin," *J. Photograph. Sci.*, **12,** 121 (1964).

Chang, L.-J., R. V. Mehta, and J. M. Tarbell, "An Evaluation of Model of Mixing and Chemical Reaction with a Turbulence Analogy," *Chem. Eng. Commun.*, **42,** 139 (1986).

Corrsin, S., "Simple Theory of an Idealized Turbulent Mixer," *AIChE J.*, **3,** 329 (1957).

Dimitt, R. L., and E. R. Graham, "Determination of Sulfate in Microgram Quantities as Barium-138 Sulfate Precipitate," *Anal. Chem.*, **48,** 604 (1976).

Fitchett, D. E., "A Study of the Effect of Mixing on the Precipitation of Barium Sulfate in a Continuous Stirred Tank Reactor, " MS Thesis, Pennsylvania State Univ. (1988).

Garside, J., and N. S. Tavare, "Mixing, Reaction and Precipitation: Limits of Micromixing in an MSMPR Crystallizer," *Chem. Eng. Sci.*, **40,** 1485 (1985).

Karpinski, P. H., "Importance of the Two-Step Crystal Growth Model," *Chem. Eng. Sci.*, **40,** 641 (1985).

Koros, W. J., D. A. Dalrymple, K. P. Kuhlman, and N. F. Brockman, "Crystallization of Sodium Chloride in a Continuous Mixed-Suspension Crystallizer," *AIChE Symp. Ser.*, **121,** 67 (1972).

Lamey, M. D., and T. A. Ring, "The Effects of Agglomeration in a Continuous Stirred-Tank Crystallizer," *Chem. Eng. Sci.*, **41,** 1213 (1986).

Levich, V. G., *Physicochemical Hydrodynamics,* Prentice-Hall, Englewood Cliffs, NJ (1962).

McCabe, W. L., "Crystal Growth in Aqueous Solutions. I-Theory," *Ind. Eng. Chem.*, **21,** 30 (1929).

Mehta, R. V., and J. M. Tarbell, "Four Environment Model of Mixing and Chemical Reaction. II: Comparison with Experiments," *AIChE J.*, **29,** 329 (1983).

Mullin, J. W., *Crystallization,* CRC Press, Cleveland, OH (1972).

Nielsen, A. E., "The Kinetics of Crystal Growth in Barium Sulfate Precipitation," *Acta. Chem. Scandia.*, **12,** 951 (1958).

——— "Homogeneous Nucleation in Barium Sulfate Precipitation," *Acta. Chem. Scandia.*, **15,** 440 (1961).

——— "Nucleation and Growth of Crystals at High Supersaturations," *Kristall. und Technik.*, **4,** 17 (1969).

Nyvlt, J., and S. Zacek, "Effect of the Role of Stirring on Crystal Size in Precipitating or Salting-out Systems," *Coll. Czech. Chem. Commun.*, **51,** 1609 (1986).

Pohorecki, R., and J. Baldyga, "The Use of a New Model of Micromixing for Determination of Crystal Size in Precipitation," *Chem. Eng. Sci.*, **38,** 79 (1983).

——— "The Effect of Micromixing on the Course of Precipitation in an Unpremixed Feed Continuous Tank Crystallizer," *5th Eur. Conf. on Mixing,* Wurzburg, W. Germany, 105 (June 10–12, 1985).

Randolph, A. D., and M. A. Larson, *Theory of Particulate Processes,* Academic Press, New York (1971).

Sano, Y., N. Yamaguchi, and T. Adachi, "Mass Transfer for Suspended Particles in Agitated Vessels and Bubble Columns," *J. Chem. Eng. Japan,* **7,** 255 (1974).

Takiyama, K., "Formation and Aging of Precipitates. A: An Electron Micro-Diffraction Study on Crystal Habit of Barium Sulfate Precipitates," *Bull. Chem. Soc. Japan,* **32,** 68 (1958).

Tarbell, J. M., and R. V. Mehta, "Mechanistic Models of Mixing and Chemical Reaction with a Turbulence Analogy," *Physicochem. Hydrodyn.*, **7,** 17 (1986).

Tsubouchi, T., and S. Sato, "Heat Transfer from Fine Wires and Particles by Natural Convection," *Chem. Eng. Prog. Symp. Ser.*, **30,** 269 (1960).

Vassilatos, G., and H. L. Toor, "Second-Order Chemical Reactions in a Nonhomogeneous Turbulent Fluid," *AIChE J.*, **11,** 666 (1965).

Villermaux, J., "Mixing in Chemical Reactors," *Am. Chem. Soc. Symp. Ser.*, **226,** 135 (1983).

Vlcek, J., I. Fort, S. Lukesova, V. Kudrna, and J. Skrivanek, "Impeller Power Consumption in a Model Crystallizer with a Cylindrical Draft Tube," *Industrial Crystallization '78,* North Holland/Elsevier, New York (1979).

Manuscript received June 14, 1989, and revision received Jan. 31, 1990.